

The formation and characterization of fretting-induced degradation layers using quenched and tempered steel

Verner Nurmi^a, Jouko Hintikka^{c,1}, Janne Juoksukangas^{a,*}, Mari Honkanen^b, Minnamari Vippola^b, Arto Lehtovaara^a, Antti Mäntylä^c, Joonas Vaara^c, Tero Frondelius^c

^a *Tribology and Machine Elements, Laboratory of Materials Science, Tampere University of Technology, P.O. Box 589, 33101 Tampere, Finland*

^b *Materials Characterization, Laboratory of Materials Science, Tampere University of Technology, P.O. Box 589, 33101 Tampere, Finland*

^c *R&D and Engineering, Wärtsilä, P.O.Box 244, 65101 Vaasa, Finland*

ARTICLE INFO

Keywords:
Fretting
Friction
Adhesion
Microscopy

ABSTRACT

Fretting movement is dangerous for machines, because it can cause cracking and surface degradation. The aim of this work was to characterize fretting-induced material degradation in large flat-on-flat contacts without edge effects in a sliding direction using quenched and tempered steel 34CrNiMo6. The focus was on the adhesive contact spots, which were formed under a wide variety of operating conditions. Characterization methods were optical microscopy, Vickers hardness tests and scanning electron microscopy. Three different degradation areas were observed: a general deformation layer, a tribologically transformed structure and a third body layer. All the degradation phases have high hardness and low ductility compared to the base material. The formation and behavior of the degradation layers in different operating conditions were discussed.

1. Introduction

In fretting, contact surfaces under normal loading will experience reciprocating relative movement. The size of this slipping movement can be anywhere between a few micrometers and several hundred micrometers. This leads to surface degradation, which also accelerates nucleation of fatigue cracks [1]. Fretting is characterized by surface damage and wear debris that tends to get trapped in the contact [2]. As fretting takes place inside the contact, there may be no discernible sign of damage before the contact is opened or the total failure of component, which is why fretting is so particularly dangerous.

Hintikka et al. [3] and Juoksukangas et al. [4] carried out fretting tests with large-scale flat-on-flat contact configurations. They observed the formation of millimeter-scale adhesive material transfer spots in their specimens of quenched and tempered steel. Hintikka also found a correspondence between these adhesive contact spots and non-Coulomb friction behavior. The coefficient of friction (COF) in a fretting contact can be easily over unity, and can thus have a decisive effect on slip and cyclic stresses. It is also worth noting that the COF can evolve during fretting tests in stable load conditions [5]. Depending on factors such as loading, contact geometry and COF, the contact can be fully sliding (gross slip), slip can occur only in certain regions (partial slip) or

the area can be completely stuck (stick). Design and dimensioning against fretting damage is challenging due to uncertainties in the friction and wear behavior in the contact [6–8].

Fretting may lead to severe changes in material microstructure and cause material transfer in the contact surfaces. Pape and Neu studied PH13-8Mo stainless steel in cylinder-on-flat and flat-on-flat contact configurations [9]. Severe plastic deformation occurred in the fretting contact and crack initiation took place within only 200 cycles. Li et al. studied fretting wear with Inconel 600 alloys in ball-on-flat contacts [10]. Cross-section samples made from the fretting scars revealed plastically deformed material (general deformation layer, GDL), extremely hard tribologically transformed structure (TTS) and a third body layer (TBL). Sauger et al. [11] proposed that TTS undergoes phase transformation leading to its thermodynamically stable microstructure, which is ferrite in the case of steels. Strain-induced recrystallization would also lead to a nanocrystalline structure. They found that most of the third body is formed when hard and brittle TTS cracks under contact stresses, milling into smaller particles, which can later sinter back to the surface forming the TBL.

Zhou et al. studied TTS in steels with a ball-on-flat fretting device [12]. TTS formation was only observed in the sliding zone, and they suggested that shear stress is the main factor for TTS formation, rather

* Corresponding author.

E-mail address: janne.juoksukangas@tut.fi (J. Juoksukangas).

¹ Formerly: Tribology and Machine Elements, Laboratory of Materials Science, Tampere University of Technology, P.O. Box 589, 33101 Tampere, Finland.

List of symbols and abbreviations

| | |
|----------|-------------------------|
| N_{LC} | loading cycles |
| p | nominal normal pressure |
| P | normal load |
| Sa | surface roughness |
| T | torque |
| u_a | sliding amplitude |
| θ | rotation |

| | |
|-----|--------------------------------------|
| BC | band contrast |
| BCC | base centered cubic |
| EBS | electron back scattering diffraction |
| EDS | energy dispersive spectrometer |
| GDL | general deformation layer |
| IPF | inverse pole figure |
| TBL | third body layer |
| TTS | tribologically transformed structure |

than temperature. Sauger et al. [13] stated that TTS formation takes place due to the accumulated plastic strain and the concentration of dislocations. They observed that the TTS contained oxygen as much as the base material, indicating that oxygen does not play a part in the generation of TTS. By evaluating the accumulated dissipated energy of a fretting contact, the threshold value needed for TTS formation can be found [11,14]. Any further increase in the dissipated energy will contribute to wear.

Colombie et al. [15] studied the formation of a debris bed in fretting and its effects on fretting wear. They concluded that in ductile metals wear particle ejection occurs after the plastic deformation of material, and that the formation of wear debris slows down the wear rate of the material. Hintikka et al. [2] obtained similar results about the effect of wear debris on wear rate in large flat-on-flat contact. Everitt et al. [16] studied the evolution of the third body in Ti-6Al-4V in a cylinder-on-flat test device. They found that in gross sliding conditions the TBL is thicker at the center of the fretting scar than it is at the edges, and the TBL is about twice as hard as the base material. Hayes and Shipway [17] studied the effect of temperature on wear in cylinder-on-flat fretting tests. A higher temperature increased the amount of sintered TBL and thus decreased the wear rate of the material.

Most fretting research utilizes Hertzian type contacts, whose contact sizes are relatively small [10,11,16]. In industrial contacts, such as bolted joints and pressure fits, the nominal contact area is typically much larger than it is in laboratory tests, and the nominal contact pressure is lower. However, there has been no coherent study of fretting-induced material behavior in nominally flat-on-flat contact surfaces over a wide range of running conditions. Therefore, the objective of this study is to characterize fretting-induced material degradation in large flat-on-flat contacts without discontinuities in a contact surface in a sliding direction using quenched and tempered steel. The study focuses on the material behavior, and on the surface layers within the vicinity of adhesive contact spots formed under a wide variety of

operating conditions. This data will contribute to our fundamental understanding of fretting damage and crack nucleation mechanisms.

2. Fretting tests

The annular flat-on-flat fretting test device that was used in the experiments is described in detail in Reference [3]. In the test device, two identical annular specimens are pressed together to form a large flat-on-flat contact without any edge effects in the sliding direction, thus efficiently simulating practical contact conditions. The test material was martensitic EN 10083-1-34CrNiMo6 + QT, which is a typical high-strength steel for machine parts under fatigue loading. Fig. 1 shows the fretting test specimen and a cross-section of the specimens and their holders. The tubular part is 5 mm thick with an inner radius of 7.5 mm and an outer radius of 12.5 mm. The surface roughness values (Sa) of the specimens were between 0.20 and 0.32 μm for all the tests.

During the experiments, normal force is kept constant while one of the specimens is rotated around its central axis to create reciprocating fretting movement between the specimens. The normal load P , torque T and rotation θ are measured, from which the coefficient of friction can be calculated [3]. The specimen's elastic deformation is included in the measurements and it is numerically removed to obtain rotation at the contact interface. Sliding between the contact surfaces is calculated using an average radius of 10 mm. Most of the tests were performed in a gross-sliding regime, but a few were also done in partial slip regime. Nominal normal pressure (p) varied from 10 to 50 MPa. The sliding amplitude in the partial slip tests was from 0.5 to 4 μm and in the gross-slip tests it was from 5 to 65 μm . The fretting loading frequency was 40 Hz. The rotation amplitude was ramped up to the desired value during the first 400 loading cycles and kept constant until the end of the test, after which the rotation amplitude was decreased to zero over 100 cycles. The tests were continued until three million load cycles was reached. Short duration tests of 100, 1000 and 10000 loading cycles

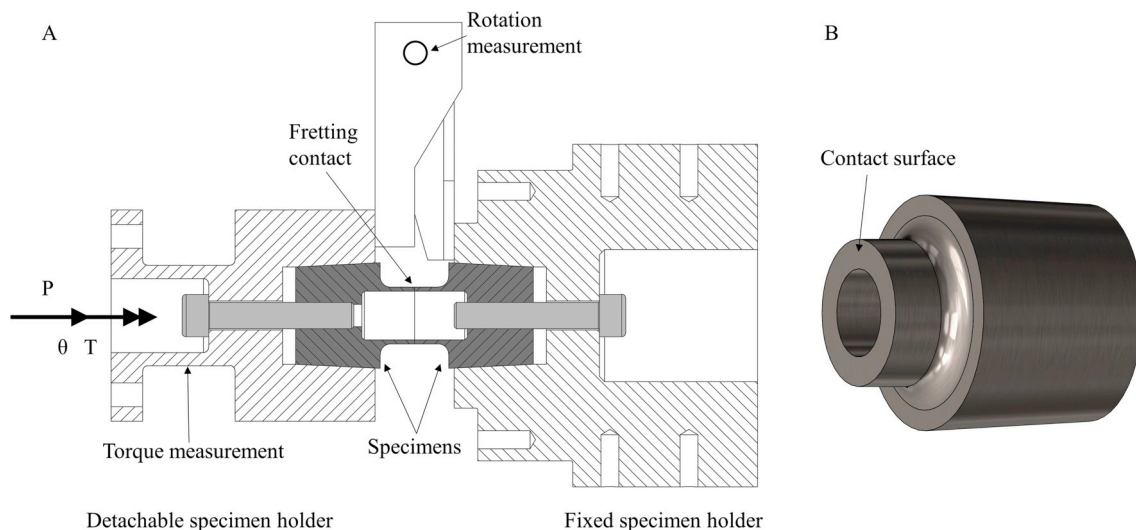


Fig. 1. Cross-section of specimens and holders (A) and test specimen (B).

Table 1
Test matrix.

| Running condition | Loading cycles N_{LC} | Normal pressure p [MPa] | Sliding amplitude u_a [μm] |
|-------------------|-------------------------|---------------------------|---|
| Gross slip | 3×10^6 | 10 | 5, 20, 35, 50, 65 |
| Gross slip | 3×10^6 | 30 | 5, 20, 35, 50, 65 |
| Gross slip | 3×10^6 | 50 | 20, 35, 50 |
| Partial slip | 3×10^6 | 30 | 0.5, 1, 2, 3, 4 |

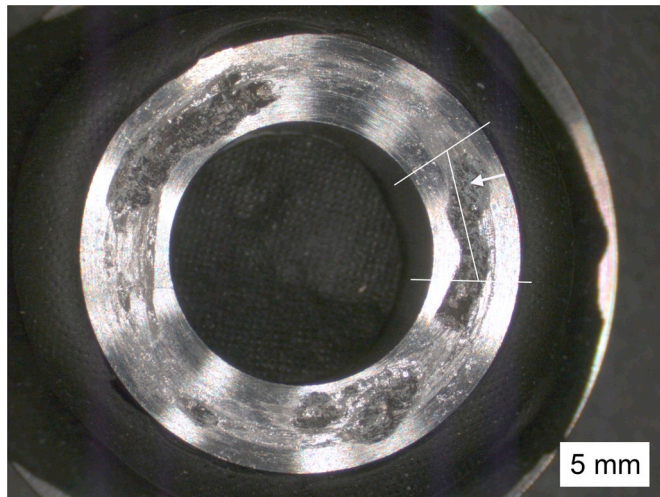


Fig. 2. The white lines represent the cutting positions. The white arrow shows the direction from which the metallurgical sample was observed.

excluding the start-up and shut-down periods were also performed. The sliding amplitude in these tests was $35\ \mu\text{m}$ and the normal pressure 30 MPa. The test conditions are summarized in Table 1.

The specimens were cleaned with solvent before the tests, thus mirroring dry contact conditions. Even distribution of the contact pressure was ensured by using pressure-sensitive paper, and contact alignment was adjusted if necessary. The full duration tests were carried out in a laboratory environment with a temperature and relative humidity between $25\text{--}30\ ^\circ\text{C}$ and $22\text{--}44\%$, respectively. The short duration tests were done at different time, when the temperature was in the range of $19\text{--}25\ ^\circ\text{C}$ and the relative humidity in the range of $14\text{--}24\%$.

3. Characterization methods

A typical contact surface with fretting scars is shown in Fig. 2, representing operating parameters of $35\ \mu\text{m}$ sliding amplitude and of 10 MPa normal pressure. The most severe fretting scars are initiated

and then spread out from the adhesion material transfer spots, hereafter referred as adhesion spots. The main point of interest in this study was the material behavior within these adhesion spots.

After the fretting tests, the procedure was first to clean the contact surfaces with acid detergent to remove loose debris from the surfaces, and then document the contact surfaces with a Leica MZ75 stereo-microscope. The cross-section samples were prepared in parallel with the slip amplitude as shown in Fig. 2. The cutting line of the cross-section sample was intended to be through the center of an adhesion spot.

The cross-section samples were mounted on a thermoset with carbon additive. The surface of the cross-section was ground and given a final polish with $1\ \mu\text{m}$ diamond suspension. After polishing, the samples were etched with 4% Nital (HNO_3) to reveal the microstructure of steel.

A Leica DM 2500 M optical microscope (OM) and a Philips XL 30 scanning electron microscope (SEM) together with an EDAX DX4 energy dispersive spectrometer (EDS) were used to document the fretting scar cross-sections. The elemental line analyses were performed with a Zeiss Crossbeam 540 SEM and an Oxford Instruments XMaxN EDS. The hardness measurements were performed with a Struers Duramin-A300 and an MMT-X7 Matsuzawa. Electron Backscatter Diffraction (EBSD) measurements were performed with a Zeiss ULTRApplus SEM, equipped with HKL Premium-F Channel EBSD system with a Nordlys F400 detector to study plastic deformation in fretting scars.

4. Results and discussion

All the fretting tests caused some degree of surface damage. The damage was most severe near the adhesion spots, which were the focus of this study. Greatest damage occurred in the samples which had suffered gross-sliding conditions and three million load cycles. As had previously been observed in the literature [10,11], there were three different degradation layers, see Fig. 3. Moving outwards from the base material to surface, these layers are the general deformation layer (GDL), the tribologically transformed structure (TTS) and the third body layer (TBL). The degree to which their properties and structure deviate from the base material follows the same in order in that; closer the layer is to the surface, the more changes the material has undergone. All three degradation phases are harder than the base material, and are discussed in more detail below in separate subsections 4.1–4.3.

The SEM studies showed no sign of plastic deformation outside immediate presence of fretting scars. According to the literature, microstructure reorientation within the grains can take place in martensite, even though no plastic deformation has occurred [18]. However, it seems that all the major changes in the material have taken place within the adhesion spots. Major cracks initiated only on the sides of the adhesion spots. Fig. 3 is a typical example. Cracks grew at an average angle of 26° measured from the contact surface. The length and

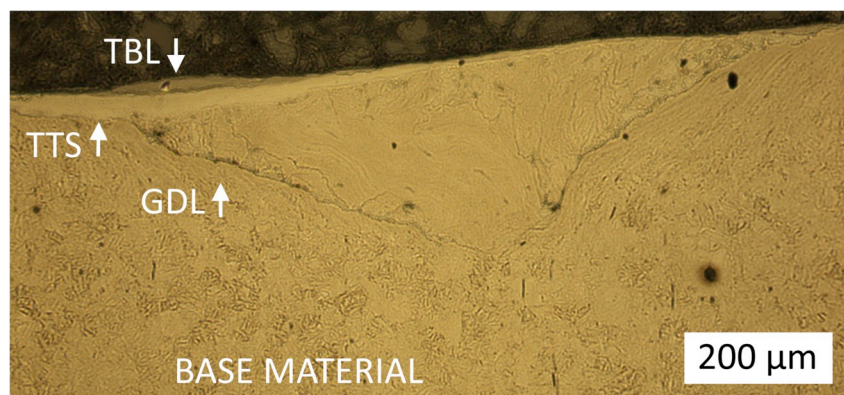


Fig. 3. Different surface layers in fretting. Test parameters: $u_a = 20\ \mu\text{m}$, $p = 30\ \text{MPa}$ and $N_{LC} = 3 \times 10^6$.

Table 2

Hardness measurement results from the base material and the GDL. The mean values and standard deviations are both higher in the deformed martensite. The measurements of the deformed martensite are made within the adhesion spots.

| Sample | Mean Value | Maximum Value | Minimum Value | Standard Deviation |
|--|------------|---------------|---------------|--------------------|
| Base Material (HV 0.05 kg) | | | | |
| 35 μm , 10 MPa, 3×10^6 | 342 HV | 382 HV | 238 HV | 39 HV |
| 35 μm , 30 MPa, 3×10^6 | 375 HV | 400 HV | 357 HV | 14 HV |
| GDL (HV 0.05 kg) | | | | |
| 50 μm , 30 MPa, 3×10^6 | 658 HV | 906 HV | 416 HV | 145 HV |
| 35 μm , 30 MPa, 3×10^6 | 517 HV | 689 HV | 384 HV | 76 HV |

Table 3

Base material composition measured with EDS.

| Base Material Composition | | | | | | | |
|---------------------------|-----|-----|-----|-----|------|-----|-------|
| Element | Si | Mo | Cr | Mn | Fe | Ni | Total |
| Wt % | 0.3 | 0.6 | 1.3 | 0.8 | 95.8 | 1.3 | 100.0 |

depth of the majority of the cracks varied from tens to hundreds of micrometers.

The material around the cracks is plastically deformed (GDL), which is essential for cracking. Farther away from the adhesion spots only the undeformed martensite (base material) and an occasional thin layer of sintered wear debris were found, the TBL being less than $5 \mu\text{m}$ thick.

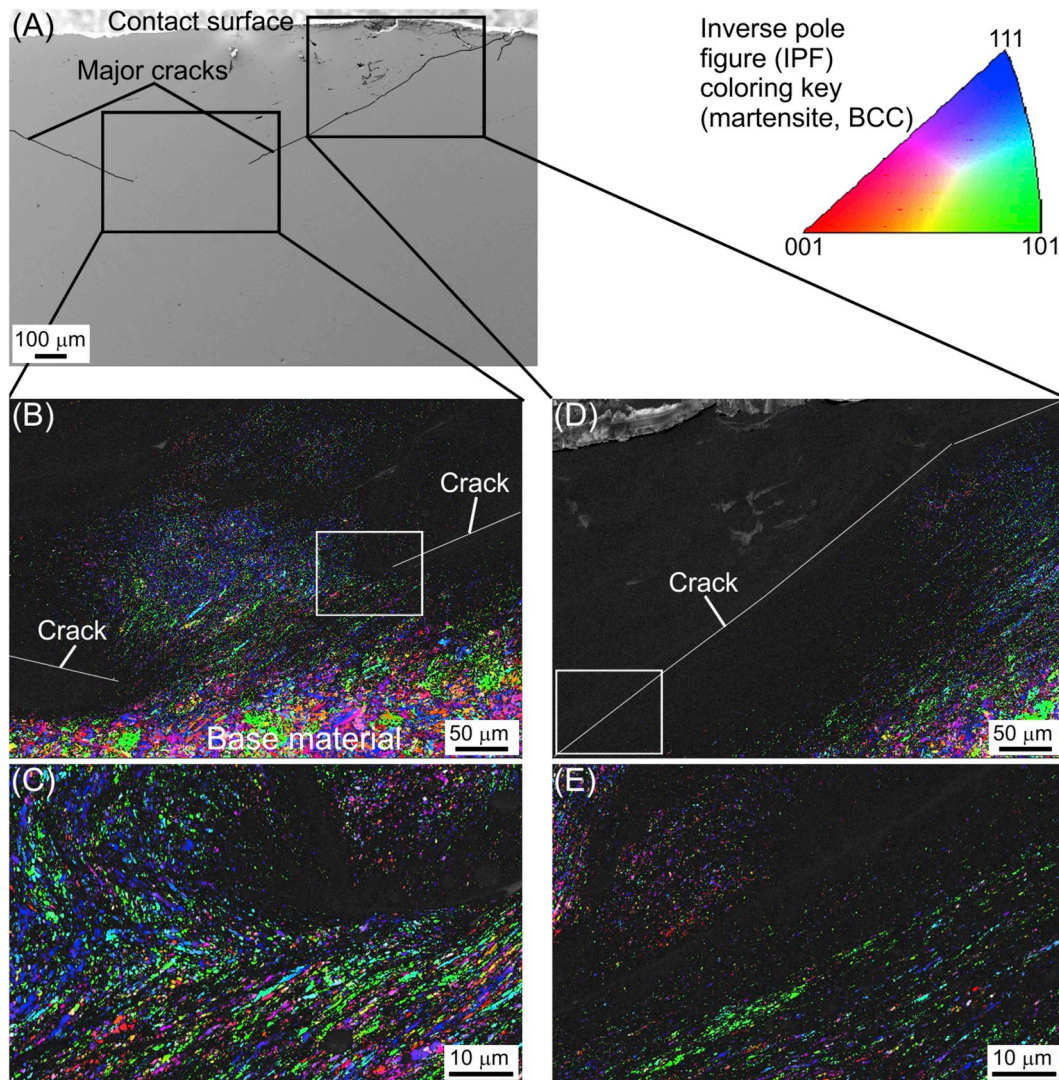


Fig. 4. SEM image (A) shows the locations of the orientation maps. The major cracks are marked by white lines. The IPF maps superimposed on the BC maps are collected from the region between the two major cracks' ends (B and C) and near the contact surface (D and E). The colors in the IPF maps correspond to the orientations (martensite, BCC) perpendicular to the observed plane as indicated by the IPF coloring key. This sample was run with test parameters of $u_a = 50 \mu\text{m}$, $p = 50 \text{ MPa}$ and $N_{LC} = 3 \times 10^6$. (For interpretation of the references to color in this figure legend, the reader is referred to the Web version of this article.)

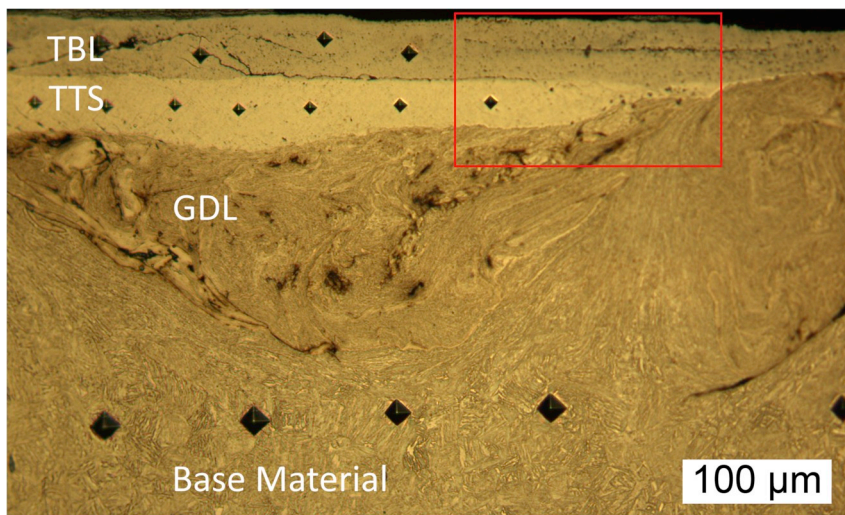


Fig. 5. Adhesion spot from a test with a sliding amplitude of 35 μm, normal pressure of 10 MPa and three million loading cycles. Extremely thick sections of both TTS and TBL occur above the crack pair. TBL is the uppermost layer, and the TTS is the lighter layer below it. The black diamonds are the Vickers hardness testing marks. The red rectangle shows the approximate location of Fig. 6 and 7. (For interpretation of the references to color in this figure legend, the reader is referred to the Web version of this article.)

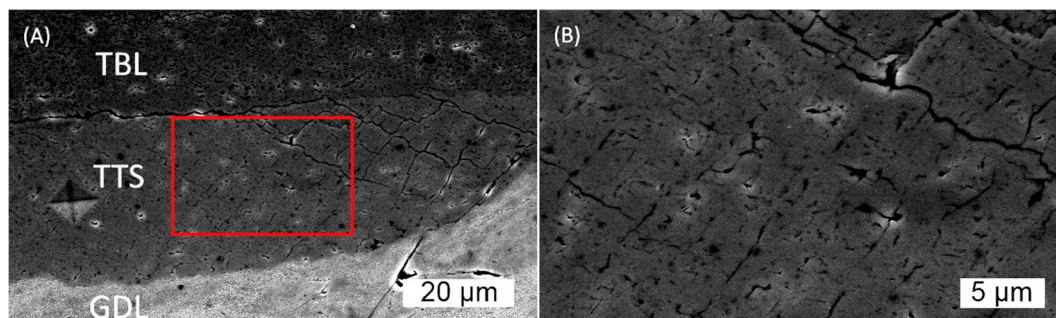


Fig. 6. SEM image of TTS layer (A). Rectangle shows location of picture B. Cracks occur everywhere in structure.

Table 4
Hardness measurements from TTS layers from different samples.

| TTS Hardness (HV 0.05 kg) | | | | |
|--------------------------------|------------|---------------|---------------|--------------------|
| u_w, p, N_{LC} | Mean Value | Maximum Value | Minimum Value | Standard Deviation |
| 35 μm, 30 MPa, 3×10^6 | 895 HV | 1036 HV | 782 HV | 90 HV |
| 35 μm, 10 MPa, 3×10^6 | 1051 HV | 1149 HV | 896 HV | 80 HV |
| 20 μm, 30 MPa, 3×10^6 | 963 HV | 1076 HV | 782 HV | 105 HV |

Table 5
Oxygen content results (EDS) from TTS in different samples. Only the oxygen contents are reported, as they the only variation from the base material. Because EDS is not a highly accurate tool for studying oxygen content, the results are rounded up or down to the closest whole percent.

| Oxygen Content of TTS | | | | |
|-----------------------|--------------------------------|----------------------|--------------------------------|---------|
| u_w, p, N_{LC} | 35 μm, 10 MPa, 3×10^6 | 35 μm, 30 MPa, 10000 | 20 μm, 30 MPa, 3×10^6 | Average |
| Wt-% | 1 | 2 | 2 | 2 |
| At-% | 4 | 6 | 7 | 6 |

4.1. General deformation layer

The general deformation layer (GDL) consists of plastically deformed martensite. The contact stresses have plastically deformed martensite making it heterogeneous in both its appearance and its mechanical properties. As can be seen in Fig. 3, the martensite under the adhesion spot is orientated parallel to the face of the crack. Table 2 presents the results of the hardness measurements of the martensite.

On average, the measured hardness values of the base material were

close to its typical values, except the minimum value of series (238 HV), which was clearly an exception. Inside the adhesion spots hardness values were 50–70% higher than in the base material. This result is interesting, because the hardness in the adhesion spots is higher than the theoretical hardness of totally work hardened material [19]. Either some phase transformations have taken place in material or compressive stresses are generated to disturb measurements [20].

Table 3 presents the elemental distribution of the steel used in our tests, measured with an SEM-EDS. The composition of the base material corresponds well to the test material's general specifications. It should be noted that the amount of carbon cannot be verified with EDS. The steel contains only small amounts of alloying materials.

EBSD measurements were used to study plastic deformation of the martensite structure within the adhesion spots and especially near the major fretting cracks. Fig. 4 shows an SEM image (Fig. 4A) from one adhesion spot showing two of the major cracks, and four normal direction inverse pole figure (IPF) orientation maps superimposed on band contrast (BC) maps (Fig. 4B–E) collected from the crack areas. The colors in the IPF map correspond to the crystallographic orientations (martensite with body-centered cubic (BCC) structure) perpendicular to the observed plane as indicated by the colored stereographic triangle,

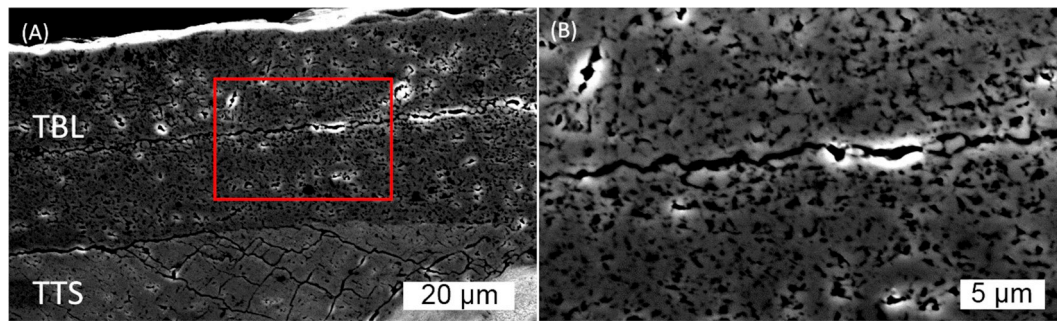


Fig. 7. SEM images from the TBL. The porosity level appears to be high. The red rectangle in (A) shows the location from which (B) is taken. The operating parameters were 35 μm slip amplitude and normal pressure of 10 MPa. (For interpretation of the references to color in this figure legend, the reader is referred to the Web version of this article.)

Table 6

TBL hardness results from three different samples.

| u_w, p, N_{LC} | Sintered Third Body Layer Hardness (HV 0.05 kg) | | | |
|--|---|---------------|---------------|--------------------|
| | Mean Value | Maximum Value | Minimum Value | Standard Deviation |
| 35 μm , 30 MPa, 3×10^6 | 748 HV | 1036 HV | 474 HV | 180 HV |
| 35 μm , 10 MPa, 3×10^6 | 676 HV | 774 HV | 384 HV | 113 HV |
| 20 μm , 30 MPa, 3×10^6 | 613 HV | 827 HV | 426 HV | 170 HV |

i.e. the IPF coloring key. The BC map represents the quality of the Kikuchi diffraction pattern for each measurement. In the BC map, white signifies that the pattern quality is good, i.e. it can be indexed and the crystal orientation can be determined (corresponding color in the IPF map). Black signifies that the pattern quality is poor, in this case because of the plastic deformation of the martensite, the presence of extremely refined martensite crystals or phase transformation. In these cases the pattern cannot be indexed as martensite BCC structure. Fig. 4D, the BC map overlaid with an IPF map, was collected near the contact surface. Based on the EBSD results, plastic deformation has occurred around the major cracks. Indexing the martensite structure has not been successful close to or above the crack, but below the crack, nearer to the base material, the level of plastic deformation is lower and indexing is possible. According to Fig. 4E, the grain size reduces near the cracks compared to the base material (Fig. 4B) and grains are orientated in the direction of the crack. Fig. 4B and C shows that the plastic deformation is less severe towards the end of the major crack. The grain size between the cracks is smaller than in the base material and some reorientation of the grains has occurred.

The EBSD results from the major crack area show that plastic deformation is severe around and between the major cracks. It strengthens the idea of cracking due to accumulated plastic strain, as has been shown in earlier research [21–24]. The level of deformation is clearly lower at the end of the crack end than it is at its initiation point in the specimen surface. In principle, the potential plastic deformation due to minor movement between crack surfaces might lead to TTS formation, but such behavior was not detected in this study. If TTS forms between crack surfaces, layer thickness would be very small. Microstructural and micromechanical modelling could be used to study plastic deformation and cracking in a fretting contact [25].

4.2. Tribologically transformed structure

Layer of the tribologically transformed structure (TTS) was found in many, but not all samples. Still, in the most gross-sliding samples the TTS layers were tens of micrometers thick. TTS always occurred within an adhesion spot. It has been suggested, that TTS formation is based on exceeding the ultimate strain level of martensite [13]. As TTS occurs within adhesion spots, this theory is totally plausible; in adhesion spots the plastic deformation level is obviously very high and the amount of

strain may exceed the ultimate strain.

Fig. 5 shows an adhesion spot, in which there are thick layers of the TTS below and the TBL above. The TTS is located above the GDL, where the plastic deformation is high. Hardness measurement marks separate the TTS from the TBL in terms of their mechanical properties. Marks in oxidized TBL behave as in typical ceramic material, where cracks are induced to corners of hardness mark. Hardness measurement marks in TTS behave more like in ductile material, and cracks are not induced to corners.

As can be seen in Fig. 6, the TTS is a highly cracked area. The cracks often run at a 45° angle to the contact surface. This kind of cracking was not detected in either the TBL or the GDL. The cracking takes place because the TTS is an extremely hard and brittle phase [13]. Fig. 6B shows a high magnification image which reveals that the cracks can occur as densely as in every micrometer.

Table 4 shows the TTS hardness measurements from three different samples. The mean values of hardness are extremely high, from 900 to 1050 HV (0.05 kg). These levels of hardness are also found in the literature, even for different materials [11]. The operating parameters do not seem to have any major effect on the hardness values, which are far higher than the hardness of totally work-hardened base material (martensite), so this indicates phase transformation. It is most likely that the strain- and dislocation-induced phase transformation takes place in a TTS, forming thermodynamically stable phases of steel, i.e., ferrite. This ferrite phase is so hard because of the nano-sized grains. As the Hall-Petch equation indicates, the reduction of grain size enhances the mechanical properties of the material [26].

In theory, the TTS's hardness could be explained by the formation of oxides, but our elemental distribution analysis showed otherwise, as seen from Table 5. The TTS has only oxidized mildly, oxygen's atomic percentage varying from 4 to 7%. Even though the EDS cannot give very accurate results about the amount of oxygen, the limited scale of the oxidation is clear and the TTS is largely composed of non-oxidized steel.

4.3. Third body layer

The highly oxidized third body layer (TBL) occurred commonly in the samples. Fig. 7 shows the TBL in the adhesion spot presented above in Fig. 5. Admittedly, this debris bed is one of the thickest found in the

Table 7
Oxygen contents from TBL of different samples.

| Oxygen Content of TBL | | | | | |
|-----------------------|---|---|---|---|---------|
| u_w, p, N_{LC} | 35 μm , 10 MPa, 3×10^6 cycles | 35 μm , 30 MPa, 10000 cycles | 20 μm , 30 MPa, 3×10^6 cycles | 20 μm , 30 MPa, 3×10^6 cycles | Average |
| Wt-% | 4 | 18 | 6 | 20 | 12 |
| At-% | 13 | 43 | 17 | 46 | 30 |

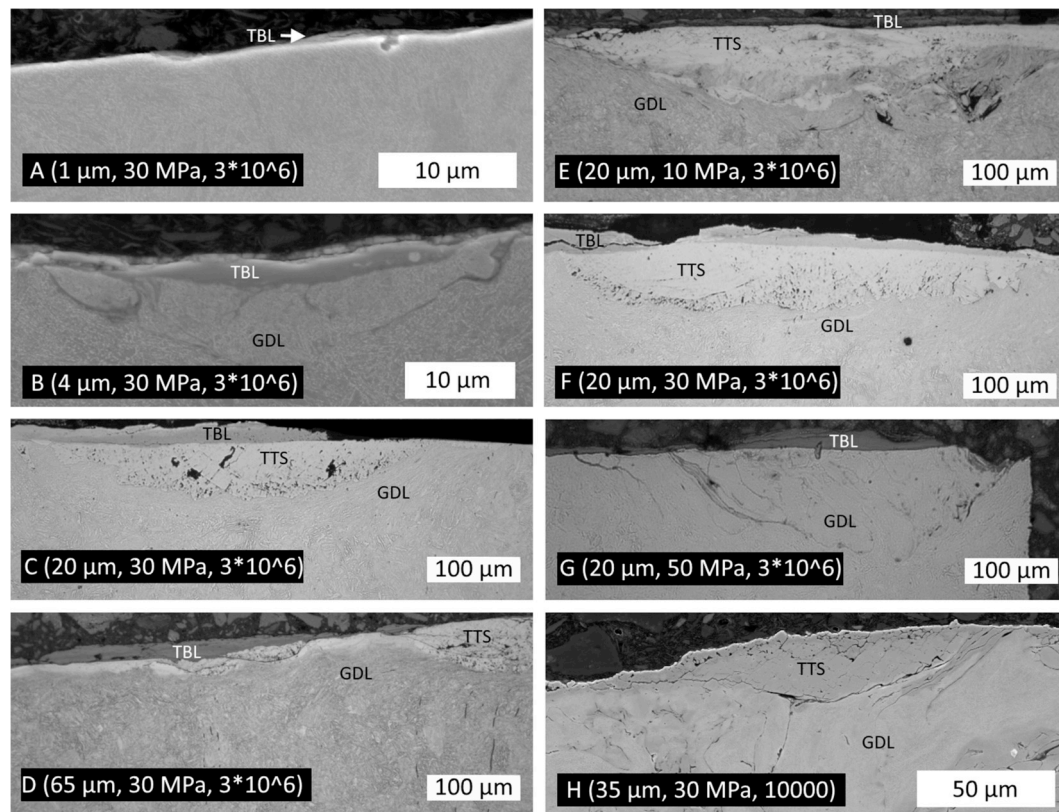


Fig. 8. Figures A to D show effect of slip amplitude on the generation of degradation layers. Lower slip amplitudes produce less TTS and TBL than higher slip amplitudes. Figures E to G show the effect of normal pressure on the generation of degradation layers. Normal pressure had no obvious effect on the generation of TTS and TBL. Figure H shows a SEM image from a short test with 10000 cycles. 10000 cycles produced a small amount of TTS, and TBL did not occur. The reader should note that the images were not taken with same magnification, and the scales are different in the images.

tests, but it is very representative in other ways. The high porosity of the layer is obvious, being the result of the third body sintering back to the contact surface. Fig. 7B also shows that the TBL is not cracked as it is in the TTS layer. Fig. 7 appears to confirm the sintering theory, as the layer consists of small, micron- and submicron-size pieces, with many pores between them. The pores form when non-compatible pieces of debris sinter together. Only small areas between single pieces adhere to each other, and pores are formed between them.

Table 6 presents the hardness values from the TBL in different samples. The mean values are from 600 to 750 HV. In theory, the hardness could be higher, but the high porosity decreases the material's mechanical properties. Nevertheless, this layer is harder than the GDL. The high standard deviation of the results (over 100 HV), can also be explained by the high porosity. As the hardness measurements were taken with a relatively low weight (0.05 kg), the diamond only leaves a small hardness mark. The porosity in that small a region can vary a lot.

Table 7 shows the measured oxygen contents (EDS) from the TBL in different samples. The variation in oxygen contents is high, between 13 and 46 atomic percent. Oxidation has most likely taken place during the stage when the third body has been unattached in the form of small particles rolling between surfaces. Other researchers have also noted variations in the oxidation level which are due to the size of the

particles and how long they have been exposed to oxygen [11].

Generally, the oxidation levels of the TBL are high, even in the shorter test of 10000 cycles. The difference between the TBL and the TTS is remarkable, and helps to explain the formation mechanisms for both layers. The TTS has had no chance to oxidize as much as the TBL. On the other hand, some areas of the TBL had the same level of oxidation as TTS. As stated above, the oxidation ratio of the TBL depends on how long the particle was loose between the surfaces and on how easily oxygen can penetrate the TBL confined between specimens. However, the hardness results and the appearance are also different, so distinguishing between these phases should not be too difficult.

4.4. Effect of the running conditions

The effect of running conditions on the occurrence of degradation layers is discussed here. Figures from 8A to 8D show the effect of slip amplitude on TTS generation. Lower slip amplitudes produce less TTS and TBL than higher slip amplitudes. All of the three-million load cycle experiments produced TTS when the slip amplitude was over 5.0 μm . In the partial slip tests (slip < 5 μm) no unambiguous observations about TTS could be made. Some thin surface layers had a fairly similar appearance, but the EDS-analyses revealed a high amount of oxygen.

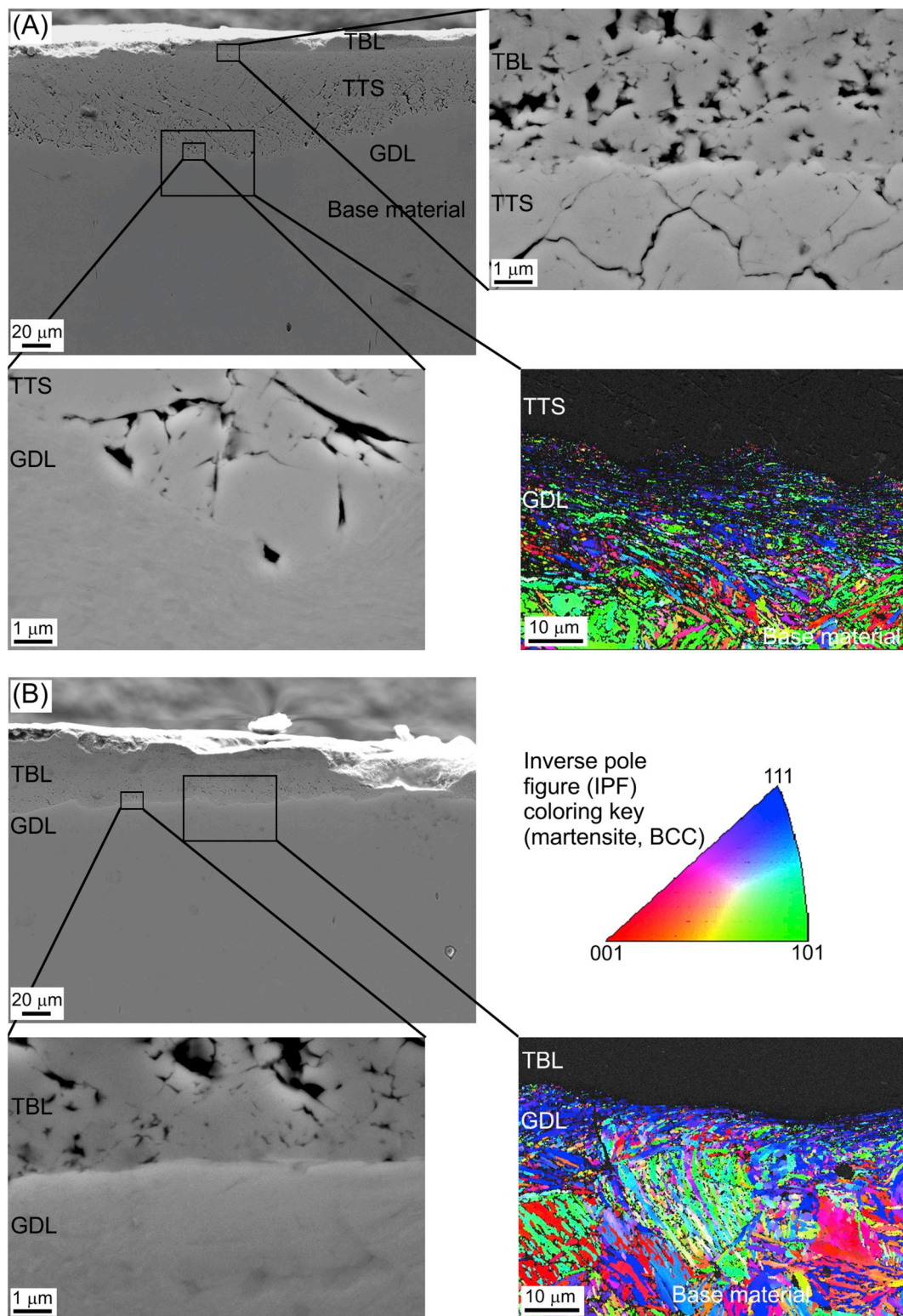


Fig. 9. (A) SEM image from the TBL-TTS and TTS-GDL interfaces and an IPF map superimposed on a BC map from the TTS-GDL interface. (B) SEM images and IPF map superimposed on a BC map from the TBL-GDL interface. The colors in the IPF maps correspond to the orientations (martensite, BCC) perpendicular to the observed plane as indicated by the IPF coloring key. (For interpretation of the references to color in this figure legend, the reader is referred to the Web version of this article.)

Hardness measurements were not performed, because the surface layers were very thin, from 2 to 5 μm. In the samples which had smaller sliding amplitude than 3 μm there was absolutely no evidence of TTS. In the gross-sliding tests, any increase in the size of the slip amplitude increased the observed amount of TTS. Indeed, in the samples which

had undergone 50 and 65 μm slip in the tests, the TTS also occurred farther away from the adhesion spot (crack pair). An increase in the sliding amplitude might increase the plastic deformation level, which is needed for TTS formation, but it also increases the dissipated energy. The formation of TTS is still not completely understood. In the future,

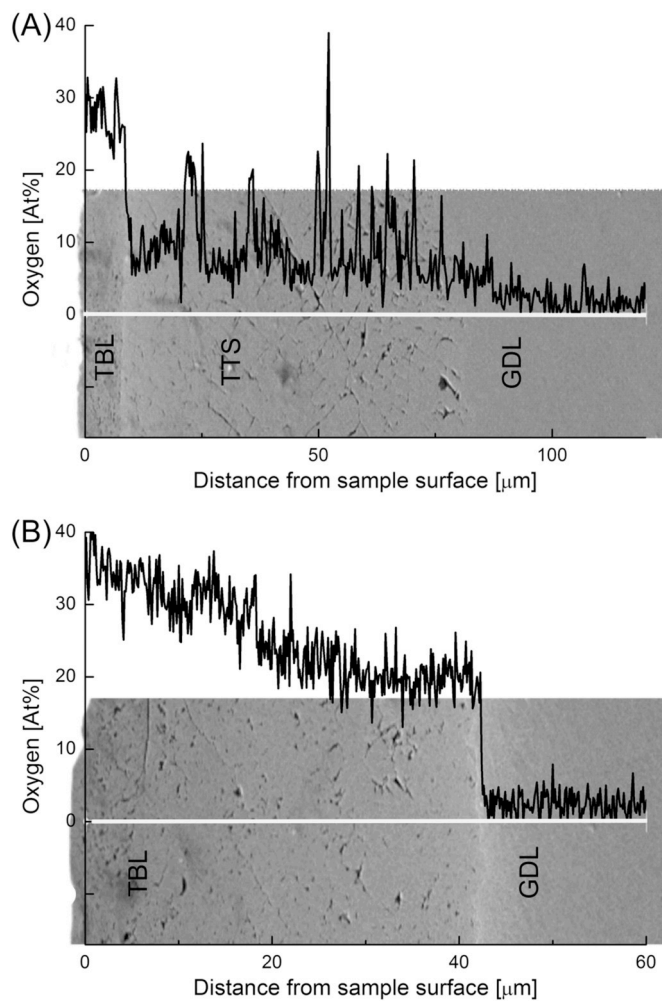


Fig. 10. EDS line analyses from the interfaces. (A) The amount of oxygen over the three layers, TBL, TTS and GDL. (B) The amount of oxygen over TBL and GDL where TTS is not present.

microstructural modelling might prove to be a vital tool for understanding this transformation, together with experimental research [27].

TTS was also found in the 10000 load cycle test, as seen in Fig. 8H. However, the cross-section sample of 1000 load cycles did not show any marks of TTS growth, even though high cracking and work hardening had taken place in the adhesion spots. Therefore, it seems that more than 1000 load cycles are needed before TTS can be observed. The amount of TTS increases with the number of load cycles, as in the 10000 load cycle test sample where it is very small. Furthermore, more plastic deformation accumulates after 10000 cycles. Fig. 8H shows TTS occurring after 10000 load cycles.

Figures from 8A to 8D show the effect of slip amplitude on TBL generation. TBL occurred even more often than TTS. The TBL was found in partial slip tests with micrometer-level slip, though it was only submicron thick and covered only small parts of the sample. There was more TBL in the partial slip tests with a slip from 3 to 4 μm, although this was still much less than what occurred in the gross-sliding tests. In the partial slip tests, the thickness of the TBL was in the micrometer scale. The gross-sliding tests produced significantly more TBL and increased the layer thickness up to several dozens of micrometers. In gross-sliding conditions, a small slip (5 μm) produced somewhat smaller amounts of TBL than a higher slip. TBL also occurred occasionally, when the test specimens had undergone a relatively low amount of load cycles. For example, the 10000 load cycle test produced a small amount of TBL. This layer was 2 μm thick.

Normal pressure did not have any obvious major effect on the generated amount of TTS or TBL. Fig. 8E and G shows this effect.

4.5. The interfaces

The interfaces between these different degradation areas tell us much about their formation mechanisms. This section studies the interfaces with conventional SEM images and EBSD measurements. The test parameters of the sample discussed below were 10 MPa nominal pressure, 35 μm sliding amplitude and three million loading cycles. All the expected degradation areas exist in the SEM image presented in Fig. 9A: TBL on the surface, TTS below it and then GDL above the base material.

The interface between the TBL and the TTS layer is clear and sharp (Fig. 9A). There is no gradual change from one phase to the other. Even though both phases are porous and cracked, they are clearly different in appearance, which indicates that they are formed differently. The interface between the TTS and the GDL is not as sharp (Fig. 9A). Although cracks may separate the two phases in some locations, in other locations the change is gradual. In the IPF map, indexing TTS according to its martensite structure was not possible due to the severe plastic deformation of the martensite, or the phase transformation from martensite to the extremely refined ferrite crystals [11]. Based on the SEM image and EBSD results, the martensite just under the TTS, i.e. the GDL, is plastically deformed and flattened in the direction of the TTS interface. Within a distance of 30 μm from the TTS-GDL interface, the martensite gradually changes from being highly deformed to the undeformed base material.

Judging from the SEM images and the EBSD results, the interface between the TBL and the GDL is sharp (Fig. 9B). In the IPF map, it was not possible to index the TBL according to martensite structure because of either severe plastic deformation or phase transformation of the martensite to extremely refined ferrite crystals. The martensite in the GDL below the TBL is less plastically transformed than it is under the TTS (Fig. 9A). At a distance of less than 10 μm from the TBL, the martensite is undeformed.

The difference between the TBL-GDL and the TTS-GDL interfaces lies in the depth and degree of the plastic deformation zone. In the TBL-GDL interface, there is a sharp change between the martensite and the TBL. The TBL is composed of sintered wear debris, so its formation on the surface does not require very high stresses. High plastic deformation is needed for the formation of the TTS, and that is why the martensite has a high degree of deformation under TTS. This is one more indication that TTS is generated by plastic strain and dislocations.

The EDS line analyses (Fig. 10) confirm the observations made about the surface layers in sections 4.3 and 4.2. In general, the TBL has a higher oxygen content nearly (30 at-%) than the TTS, whose oxygen content is below 10 at-% (Fig. 10A). In the TTS layer, there are noticeably high oxygen peaks in some of the surface cracks due to the remaining colloidal oxygen-containing silica suspension used for the final polishing of the SEM sample. In the GDL, the oxygen level is generally slightly lower (< 5 at-%) than it is in the TTS and there are no high peaks because there are no cracks. In the interface between the TBL and the GDL (Fig. 10B), the oxygen content drops from high (~30 at-%) to low (~2 at-%).

5. Conclusions

The objective of this study was to characterize fretting induced material changes and damage formation within the adhesion spots which appear in large scale flat-on-flat contacts. Three different degradation areas were observed as follows: the general deformation layer (GDL), the tribologically transformed structure (TTS) and the third body layer (TBL). All the degradation phases have high hardness and low ductility compared to the base material (martensite). Earlier studies with small scale ball-on-flat contacts have observed similar kinds of

surface layers.

The formation of the TTS layer with high hardness occurs on the surface of the adhesion spot or in its immediate vicinity. Slip was found to be essential for TTS formation, as higher slip produced more extensive TTS layer. With a contact pressure of 30 MPa and a sliding amplitude of 35 μm , TTS was observed to develop already between 1000 and 10000 load cycles. The nominal contact pressure has no major effect on the TTS layer in the range of 10–50 MPa; however true stresses and strains within the adhesion spot may well play a role in formation of the TTS.

The third body layer is the result of wear and the sintering process in fretting. This layer has high porosity and there are large variations in its high hardness. TBL occurred in all the measured gross-sliding conditions, and it increased as the slip amplitude increased. The partial slip samples contained far less TBL, and no TBL occurred after 10000 load cycles in gross-sliding conditions. The TBL can be distinguished from the TTS layer due to its clearly higher levels of oxygen and porosity.

In the GDL, severe plastic deformation occurred in the adhesion spots, the level of deformation being higher the nearer it was to the contact surface. The martensite is reoriented and the grains flattened along in the direction of the major cracks, which reinforces the idea of the crack initiation due to accumulated plastic strain.

The interface between the TBL and the martensite is sharp, and shows that the martensite has undergone only minor deformations, staying much like the base material. The interface between the GDL and the TTS is not as sharp. Although cracks separate the two phases in many locations, in other locations the change is gradual. The martensite immediately below the TTS is plastically deformed and flattened in the direction of the TTS interface.

Acknowledgements

The authors are grateful for the financial support provided by Business Finland Oy (former Tekes) in the form of a research project WIMMA Dnro 1566/31/2015 and Wärtsilä Finland Oy.

References

- [1] Wallace JM, Neu R. Fretting fatigue crack nucleation in Ti–6Al–4V. *Fatig Fract Eng Mater Struct* 2003;26(3):199–214 <https://doi.org/10.1046/j.1460-2695.2003.00553.x>.
- [2] Hintikka J, Lehtovaara A, Mäntylä A. Third particle ejection effects on wear with quenched and tempered steel fretting contact. *Tribol Trans* 2017;60(1):70–8 <https://doi.org/10.1080/10402004.2016.1146813>.
- [3] Hintikka J, Lehtovaara A, Mäntylä A. Fretting-induced friction and wear in large flat-on-flat contact with quenched and tempered steel. *Tribol Int* 2015;92:191–202 <https://doi.org/10.1016/j.triboint.2015.06.008>.
- [4] Juoksukangas J, Lehtovaara A, Mäntylä A. Experimental and numerical investigation of fretting fatigue behavior in bolted joints. *Tribol Int* 2016;103:440–8 <https://doi.org/10.1016/j.triboint.2016.07.021>.
- [5] Hintikka J, Lehtovaara A, Frondelius T, Mäntylä A. Tangential traction instability in fretting contact below fully developed friction load. *Rakenteiden mekaniikka* 2017;50(3):175–8 <https://doi.org/10.23998/rm.65105>.
- [6] Hintikka J, Juoksukangas J, Lehtovaara A, Frondelius T, Mäntylä A. Non-idealities in fretting contacts. *Rakenteiden Mekaniikka* 2017;50(3):171–4 <https://doi.org/10.23998/rm.64886>.
- [7] Waterhouse RB. *Fretting corrosion*. tenth ed. Oxford: Pergamon Press; 1972. p. 253.
- [8] Hills DA. Mechanics of fretting fatigue. *Wear* 1994;175(1–2):107–13 [https://doi.org/10.1016/S0043-1648\(94\)90173-2](https://doi.org/10.1016/S0043-1648(94)90173-2).
- [9] Pape J, Neu R. Fretting fatigue damage accumulation in PH13–8Mo stainless steel. *Int J Fatig* 2001;23:437–44 [https://doi.org/10.1016/S0142-1123\(01\)00140-2](https://doi.org/10.1016/S0142-1123(01)00140-2).
- [10] Li J, Lu Y, Zhang H, Xin L. Effect of grain size and hardness on fretting wear behavior of Inconel 600 alloys. *Tribol Int* 2015;81:215–22 <https://doi.org/10.1016/j.triboint.2014.08.005>.
- [11] Sauger E, Fouvry S, Ponnsonnet L, Kapsa P, Martin J, Vincent L. Tribologically transformed structure in fretting. *Wear* 2000;245(1):39–52 [https://doi.org/10.1016/S0043-1648\(00\)00464-6](https://doi.org/10.1016/S0043-1648(00)00464-6).
- [12] Zhou Z, Sauger E, Liu J, Vincent L. Nucleation and early growth of tribologically transformed structure (TTS) induced by fretting. *Wear* 1997;212(1):50–8 [https://doi.org/10.1016/S0043-1648\(97\)00141-5](https://doi.org/10.1016/S0043-1648(97)00141-5).
- [13] Sauger E, Ponnsonnet L, Martin J, Vincent L. Study of the tribologically transformed structure created during fretting tests. *Tribol Int* 2000;33(11):743–50 [https://doi.org/10.1016/S0301-679X\(00\)00088-8](https://doi.org/10.1016/S0301-679X(00)00088-8).
- [14] Fouvry S, Liskiewicz T, Kapsa P, Hannel S, Sauger E. An energy description of wear mechanisms and its applications to oscillating sliding contacts. *Wear* 2003;255(1–6):287–98 [https://doi.org/10.1016/S0043-1648\(03\)00117-0](https://doi.org/10.1016/S0043-1648(03)00117-0).
- [15] Colombie C, Berthier Y, Floquet A, Vincent L, Godet M. Fretting: load carrying capacity of wear debris. *J Tribol* 1984;106(2):194–201 <https://doi.org/10.1115/1.3260881>.
- [16] Everitt N, Ding J, Bandak G, Shipway P, Leen S, Williams E. Characterisation of fretting-induced wear debris for Ti-6Al-4 V. *Wear* 2009;267(1):283–91 <https://doi.org/10.1016/j.wear.2008.12.032>.
- [17] Hayes E, Shipway P. Effect of test conditions on the temperature at which a protective debris bed is formed in fretting of a high strength steel. *Wear* 2017;376:1460–6 <https://doi.org/10.1016/j.wear.2017.01.057>.
- [18] Swalla DR, Neu RW, McDowell DL. Microstructural characterization of Ti-6Al-4V subjected to fretting. *Trans.-Am. Soc. Mech. Eng. J. Tribol.* 2004;126:809–16 <https://doi.org/10.1115/TRIB2004-64011>.
- [19] Pavlina E, Van Tyne C. Correlation of yield strength and tensile strength with hardness for steels. *J Mater Eng Perform* 2008;17(6):888–93 <https://doi.org/10.1007/s11665-008-9225-5>.
- [20] Huber N, Heerens J. On the effect of a general residual stress state on indentation and hardness testing. *Acta Mater* 2008;56(20):6205–13 <https://doi.org/10.1016/j.actamat.2008.08.029>.
- [21] Zhou Z, Vincent L. Mixed fretting regime. *Wear* 1995;181:531–6 [https://doi.org/10.1016/0043-1648\(95\)90168-X](https://doi.org/10.1016/0043-1648(95)90168-X).
- [22] Basseville S, Cailletaud G. An evaluation of the competition between wear and crack initiation in fretting conditions for Ti–6Al–4V alloy. *Wear* 2015;328:443–55 <https://doi.org/10.1016/j.wear.2015.03.010>.
- [23] Jeung H, Kwon J, Lee CY. Crack initiation and propagation under fretting fatigue of inconel 600 alloy. *J Mech Sci Technol* 2015;29(12):5241–4 <https://doi.org/10.1007/s12206-015-1124-8>.
- [24] Wang J, Xu H, Su T, Zhang Y, Guo Z, Mao H, Zhang Y. Fretting fatigue experiment and analysis of AlSi9Cu2Mg alloy. *Materials* 2016;9(12):984 <https://doi.org/10.3390/ma9120984>.
- [25] Laukkanen A, Lindroos M, Andersson T, Verho T, Pinomaa T. Micromechanical modeling of failure behavior of metallic materials. *Rakenteiden Mekaniikka* 2017;50(3):271–4 <https://doi.org/10.23998/rm.65161>.
- [26] Callister WD, Rethwisch DG. *Materials science and engineering*. NY: John Wiley & Sons; 2011.
- [27] Sippola MK, Laukkanen A, Andersson T, Lindroos M. Microstructural modelling of materials. *Rakenteiden Mekaniikka* 2017;50(3):256–60 <https://doi.org/10.23998/rm.65075>.